ACS APPLIED MATERIALS & INTERFACES

Research Article

www.acsami.org

Rhodium-Doped Barium Titanate Perovskite as a Stable p-Type Semiconductor Photocatalyst for Hydrogen Evolution under Visible Light

Kazuhiko Maeda*

Department of Chemistry, Graduate School of Science and Engineering, Tokyo Institute of Technology, 2-12-1-NE-2 Ookayama, Meguro-ku, Tokyo 152-8550, Japan

Precursory Research for Embryonic Science and Technology (PRESTO), Japan Science and Technology Agency (JST), 4-1-8 Honcho Kawaguchi, Saitama 332-0012, Japan

Supporting Information

ABSTRACT: Rhodium-doped barium titanate ($BaTiO_3$:Rh) powder was prepared by the polymerized complex (PC) method, and the photocatalytic activity for H_2 evolution from water was examined. $BaTiO_3$ is a wide-gap n-type semiconductor having a band gap of 3.0 eV. Doping Rh species into the lattice of $BaTiO_3$ resulted in the formation of new absorption bands in visible light region. Upon visible light ($\lambda >$ 420 nm), $BaTiO_3$:Rh modified with nanoparticulate Pt as a water reduction promoter was capable of producing H_2 from water containing an electron donor such as methanol and iodide. The best material prepared by the PC method exhibited higher activity than that made by a conventional solid-state reaction method. Visible-light-driven Z-scheme water splitting was also accomplished using Pt/$BaTiO_3$:Rh as a building block for H_2 evolution in combination with PtO_x-loaded WO_3 as an O_2 evolution photocatalyst in the presence of an IO_3^-/I^- shuttle redox mediator. Photoelectrochemical analysis indicated that a porous $BaTiO_3$:Rh electrode exhibited cathodic photoresponse due to water reduction in a neutral aqueous Na_2SO_4 solution upon visible light.

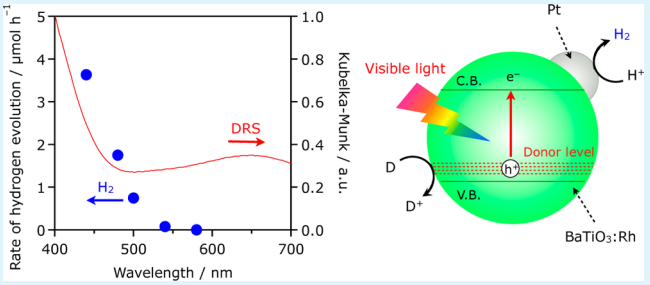

KEYWORDS: *artificial photosynthesis, doping, perovskite, photocathode, solar energy conversion, Z-scheme*

1. INTRODUCTION

Visible-light water splitting using a heterogeneous photocatalyst has drawn attention from the viewpoint of solar hydrogen production from renewable resources in large-scale.[1−5] One of the most important subjects in this research area is to develop a photocatalyst that is active for H_2 evolution under visible light and is applicable to a nonsacrificial water splitting system such as Z-scheme.[1,5] Although various systems based on metal-oxides[6−14] and oxynitrides[15−21] have been proposed to do this job, none have yielded a satisfactory result.

Doping a foreign element into a wide-gap oxide semiconductor as a host material is a well-known approach to produce a visible-light-driven photocatalyst.[1] Wide gap metal oxides, which are active for overall water splitting, such as TiO_2, $SrTiO_3$, $La_2Ti_2O_7$, $CaTiO_3$, $NaTaO_3$, and $ZnGa_2O_4$ have dominantly been employed as host materials.[22−29] The doped element in such a wide gap metal oxide works as a center of visible-light absorption by making a donor or acceptor level, depending on dopants. Among the dopants examined, Rh has been reported to be one of the most effective ones to activate $SrTiO_3$ for H_2 evolution.[1,25] Follow-up studies have indicated that several metal oxides doped with Rh exhibited certain visible-light activity for H_2 evolution from water containing a sacrificial electron donor like methanol.[27,29] However, it should be stressed that there are very few metal oxides (not only doped oxides but also undoped ones) that achieve the functionality as a visible-light-responsive H_2 evolution photocatalyst for "nonsacrificial" Z-scheme water splitting; only $SrTiO_3$-based doped materials ($SrTiO_3$:Rh and $SrTiO_3$:Cr/Ta) and coumarin-adsorbed $H_2K_2Nb_6O_{17}$ have been reported to serve as active H_2 evolution photocatalysts in the presence of a suitable shuttle redox mediator.[6−14]

Another interesting aspect of Rh doping into an n-type semiconductor oxide like $SrTiO_3$ is that it may produce a new p-type semiconductor, which is potentially useful for various applications in water-splitting photoelectrochemical cell, solar cells and so on.[30] Regarding water-splitting photoelectrode, although many n-type oxide semiconductors have been reported,[3] the number of stable p-type metal oxides is limited.[31,32] Therefore, the development of a new metal-oxide that photocatalytically produces H_2 from water and exhibits p-

Received: November 22, 2013
Accepted: January 10, 2014
Published: January 10, 2014

   dx.doi.org/10.1021/am405293e | ACS Appl. Mater. Interfaces 2014, 6, 2167−2173

type semiconducting property remains an important mission in the field of photochemical water-splitting research.

In this study, $BaTiO_3$, a wide-gap metal oxide having perovskite structure, was chosen as the host material to prepare a doped photocatalyst capable of reducing water with visible light. From the standpoint of photocatalyst preparation, more homogeneous distribution of dopants in a metal oxide appears to be preferable for making an efficient photocatalyst based on doping. The polymerized complex (PC) method, originally developed by Pechini,[33] is a powerful and convenient technique that allows for the synthesis of crystalline complex metal oxides even at reduced temperature. Although the effectiveness of the PC method have been shown in the synthesis of a number of metal oxides for overall water splitting,[1] the applicability of this method to the synthesis of doped metal oxide has rarely been investigated so far.

This paper reports the preparation of Rh-doped $BaTiO_3$ powder by the PC method, and demonstrates the functionality of the material as a visible-light-driven photocatalyst for H_2 evolution from water even in a non-sacrificial manner. Photoelectrochemical property of Rh-doped $BaTiO_3$ for water splitting is also examined.

2. EXPERIMENTAL SECTION

2.1. Preparation of Photocatalysts. $BaTiO_3$ doped with Rh was prepared by the polymerized complex (PC) method by a variation of the procedure reported by Kakihana et al.[34] An appropriate amount of titanium tetra-isopropoxide (97.0%; Kanto Chemicals), 1.2 mol of ethylene glycol (EG) (99.5%; Kanto Chemicals), and 0.3 mol of anhydrous citric acid (CA) (98.0%; Wako Pure Chemicals) were added into a methanol solution (100 mL, ≥99.5%; Kanto Chemicals) to make a transparent solution. Then, an appropriate amount of $RhCl_3{\cdot}3H_2O$ (99.5%; Wako Pure Chemicals) was added into the solution. After complete dissolution, 30 mmol of $BaCO_3$ (99.0%; Kanto Chemicals) was added and dissolved into the solution. The ratio of Rh to the total amount of Ti and Rh (30 mmol) varied from 0 to 5.0 mol %. The as-prepared solution was heated at ca. 400 K to achieve complete dissolution and promote esterification between EG and CA, yielding a glassy resin. The resin was then calcined at ca. 673 K in a mantle heater to complete decomposition. The resulting black powder was subsequently calcined on an Al_2O_3 plate at 823 K for 5 h in air to remove the carbon-containing species. Finally, the resulting powder was collected and heated in air at 1273 K for 2 h in an Al_2O_3 crucible (ramp rate, 10 K min^{-1}).

For comparison, $BaTiO_3$:Rh (1.0 mol %) was prepared by a conventional SSR method. 30 mmol of $BaCO_3$, 29.7 mmol of TiO_2 (99.0%, rutile form; Kanto Chemicals), and 0.15 mmol of Rh_2O_3 (98.0−102.0%; Wako Pure Chemicals) were mixed vigorously in a small amount of methanol using an agate mortar and a pestle. The mixture was subject to heating in air at 1123 K for 1 h (ramp rate, 10 K min^{-1}). After cooling down the temperature, the mixture was grinded, and heated again in a similar manner at 1273 K for 10 h.

For Z-scheme water splitting, PtO_x-loaded WO_3 (0.5 wt % Pt as a metal basis) was employed as an O_2 evolution photocatalyst.[7,35] The detailed preparation procedure can be found in the previous literatures.[7,35]

2.2. Preparation of Electrodes. A porous $BaTiO_3$:Rh electrode was prepared by pasting a viscous slurry onto conducting glass according to a method described previously with some modifications.[36] A mixture of 0.1 g of the as-prepared $BaTiO_3$:Rh powder, 10 μL of acetylacetone (Kanto Chemicals), 10 μL of TritonX (Aldrich, USA), 10 μL of poly(ethylene glycol) 300 (Kanto Chemicals), and 1000 μL of distilled water was ground in an agate mortar for preparation of the viscous slurry. The slurry was then pasted on fluorine-doped tin-oxide (FTO) glass slides (thickness 1.5 mm; Asahi Glass, Japan) to prepare a 1.5 × 3.5 cm^2 electrode, and the sample was calcined in air at 723 K for 1 h.

2.3. Characterization of Catalysts. The samples prepared were studied by powder X-ray diffraction (XRD; MiniFlex 600, Rigaku; Cu Kα), scanning electron microscopy (SEM; S-4700, Hitachi), UV-visible diffuse reflectance spectroscopy (DRS; V-565, JASCO), and X-ray photoelectron spectroscopy (XPS; ESCA-3200, Shimadzu). The Brunauer−Emmett−Teller (BET) surface area was measured using a BELSORP-mini (BEL Japan) at liquid nitrogen temperature (77 K). The binding energies determined by XPS were corrected by reference to the C 1s peak (284.6 eV) for each sample.

2.4. Photocatalytic Reactions. Reactions were carried out in a Pyrex top-irradiation vessel connected to a glass closed gas circulation system. Photoreduction of water was performed by dispersing 100 mg of the as-prepared powder in an aqueous methanol solution (10 vol%, 100 mL) as an electron donor. A cocatalyst, 0.25 wt % Pt, was loaded in-situ onto the as-prepared $BaTiO_3$:Rh using H_2PtCl_6 as the precursor,[37] unless otherwise stated. For Z-scheme water splitting, 25 mg of the Pt-loaded sample and 50 mg of PtO_x/WO_3 were dispersed in an aqueous NaI (Reagent grade, Kanto Chemicals) solution (10 mM, 100 mL). The reactant solution was evacuated several times to remove air completely, and a small amount of Ar gas (ca. 5 kPa) was introduced into the reaction system prior to irradiation under a 300 W xenon lamp (Cermax, PE300BF) with an output current of 20 A unless otherwise stated. The irradiation wavelength was controlled by the combination of a cold mirror (CM-1), cutoff filter (L-42) and water filter (λ > 420 nm). To examine the dependence of the cutoff wavelength of incident light on activity, another cutoff filter was fitted in addition to the L-42 filter, with a xenon lamp output current of 10 A. The reactant solution was maintained at room temperature by a water bath during the reaction. The evolved gases were analyzed by gas chromatography (Shimadzu, GC-8A with TCD detector and MS-5A column, argon carrier gas).

Apparent quantum yields (AQYs) for water reduction were measured using the same experimental setup, except for the addition of a band pass filter (λ = 420.5 nm), and were estimated by the equation

$$\mathrm{AQY}(\%) = AR/I \times 100 \quad (1)$$

where A, R, and I represent the coefficient based on the reaction (H_2 evolution, 2), the H_2 evolution rate, and the rate of incident photons, respectively. The total number of incident photons (ca. 150 mW) was measured using a calibrated silicon photodiode. The reproducibility of the gas evolution rate was typically within ∼10% under a given set of reaction conditions.

2.5. Photoelectrochemical Measurements. Photoelectrochemical measurements were carried out with a potentiostat (HSV-110, Hokuto Denko) and an electrochemical cell at room temperature. The cell was made of Pyrex glass, and was a three electrode-type system using a Pt wire and Ag/AgCl electrode as the counter and reference electrodes, respectively. An aqueous Na_2SO_4 solution (pH = 5.9) was used as the electrolyte, which was saturated with argon gas prior to the electrochemical measurements. Visible light irradiation (λ > 420 nm) was conducted from the backside of the working electrode, with a xenon lamp (300 W) as light source, fitted with a cold mirror (CM-1) and a cutoff filter.

3. RESULTS AND DISCUSSION

3.1. Structural Characterization. Figure 1 shows XRD patterns of samples prepared by the PC method. All of the prepared samples, except for the 5.0 mol % Rh-doped sample, had single-phase diffraction patterns identical to that of perovskite $BaTiO_3$ without any impurity phase. The positions of the diffraction peak tended to shift to lower 2θ angles with increasing Rh doping amount. This is reasonable, considering the difference in ionic radius with a six coordination number between Ti^{4+} and Rh^{3+}.[38] In addition, the shape of diffraction pattern of $BaTiO_3$ changed with Rh doping. In the 5.0 mol % doping sample, the main peak was again split into two, whose shape was different from the original asymmetric shape of

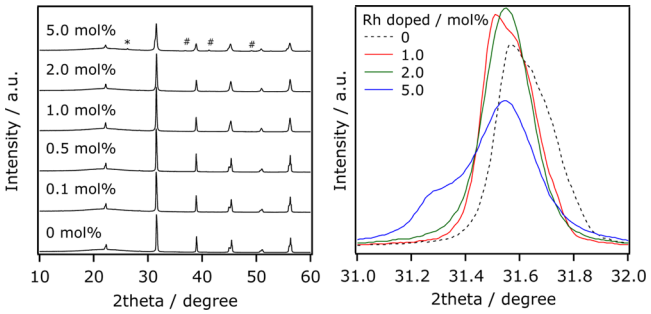

Figure 1. XRD patterns of samples prepared by the PC method with different Rh doping amounts. * and # indicate peaks derived from $Ba_9Rh_8O_{24}$ and unidentified compounds.

$BaTiO_3$, indicative of inhomogeneous doping of Rh at higher doping concentration. Nevertheless, these observations clearly show that Rh species are successfully incorporated into the lattice of $BaTiO_3$.

The particle morphology of the same samples was examined by means of SEM, which indicated that the samples consisted of aggregated particles with a primary particle size of 100−400 nm (Figure 2). The primary particle size remained almost unchanged up to 1.0 mol % Rh doping, but gradually decreased with increasing the doping amount from 1.0 to 5.0 mol %. This is consistent with the change in specific surface areas of the same samples, as listed in Table 1.

Figure 3 shows diffuse reflectance spectra of Rh-doped $BaTiO_3$ samples. Undoped $BaTiO_3$ exhibited an absorption edge at around 400 nm, assignable to electron transitions from the valence band formed by O2p orbitals to the conduction band consisting of empty 3d orbitals of Ti. On the other hand, Rh-doped $BaTiO_3$ samples have two absorption bands in visible light region (400−800 nm) in addition to the original band gap transition of the host compound at 400 nm. The intensities of these visible light absorption bands become stronger with increasing the concentration of doped Rh without changing the absorption edge of the host compound.

Table 1. Specific Surface Areas and Photocatalytic Activities of $BaTiO_3$:Rh for H_2 Evolution from an Aqueous Methanol Solution under Visible Light (λ > 420 nm)[a]

entry	preparation method	amount of Rh doped (mol %)	specific surface area ($m^2\ g^{-1}$)	H_2 evolution rate ($\mu mol\ h^{-1}$)
1	PC	0	3.3	0.8
2	PC	0.1	3.1	1.0
3	PC	0.5	3.0	6.4
4	PC	1.0	3.2	30.8
5	PC	2.0	4.6	24.1
6	PC	5.0	6.4	19.9
7	SSR	1.0	2.0	4.8

[a]Reaction conditions: catalyst, 100 mg (0.25 wt % Pt photodeposited in-situ); 10 vol % aqueous methanol solution 100 mL; light source, xenon lamp (300 W) fitted with a cold mirror (CM-1) and a cutoff filter (L42); reaction vessel, Pyrex top-irradiation type.

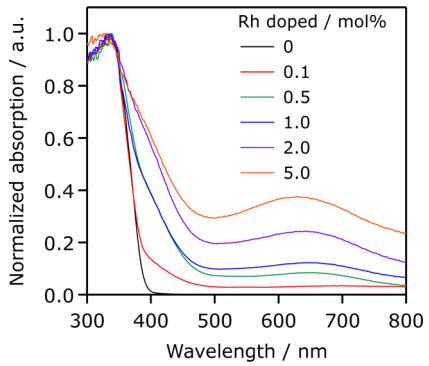

Figure 3. DRS of $BaTiO_3$ doped with different amounts of Rh. Samples were prepared by the PC method.

It has been reported by Kudo et al.[23,25] that doped Rh^{3+} species in metal oxides such as $SrTiO_3$ and TiO_2 give a relatively steep absorption at 500−600 nm that results from electron transitions from a donor level formed by Rh^{3+} in the forbidden band of the host compound to the conduction band

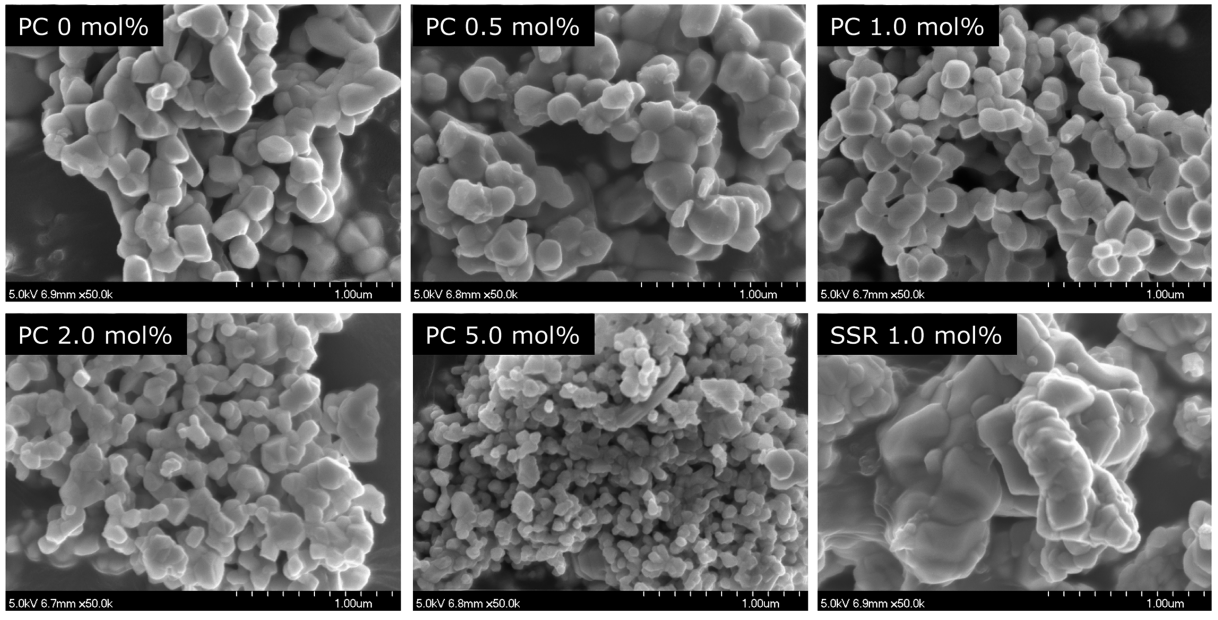

Figure 2. SEM images of $BaTiO_3$ doped with different amounts of Rh. Samples were prepared by either the polymerized complex (PC) method or solid-state reaction (SSR) method.

dx.doi.org/10.1021/am405293e | ACS Appl. Mater. Interfaces 2014, 6, 2167−2173

consisting of empty Ti3d orbitals. On the other hand, Rh^{4+} species exhibit a broad absorption extended to near infrared region. Therefore, the absorption edge at around 500 nm can be assigned to Rh^{3+} species while another absorption band observed at 700 nm is attributable to Rh^{4+} species. To obtain further insight on the oxidation state of doped Rh species in $BaTiO_3$, $BaTiO_3$:Rh was subject to reduction with H_2 gas at 573 K for 1 h. As shown in Figure S1A in the Supporting Information, the absorption band centered at 660 nm disappeared after the H_2-reduction treatment. This result supports the above-mentioned assignment.

On the basis of these results, Rh-doped $BaTiO_3$ samples were successfully prepared by the PC method, and the doped Rh species was suggested to have at least two oxidation numbers of Rh^{3+} and Rh^{4+}. The characteristic oxidation state of Rh in $BaTiO_3$:Rh is similar to that in $SrTiO_3$:Rh.[25] To further obtain information on the valence state of Rh, XPS measurements were conducted. As shown in Figure S1B in the Supporting Information, the $Rh3d_{5/2}$ peak for the as-prepared sample appears at around 308.5 eV, which is assigned to trivalent Rh species.[39,40] The spectral shape remained largely unchanged even after H_2-reduction treatment. This seems to contradict the results of DRS measurements, which showed that the as-prepared sample contained both trivalent and tetravalent Rh species, while the H_2-treated sample exhibited only trivalent Rh feature. Presumably, the change in the state of the surface Rh species between the two samples was too small to be detected by XPS measurements, as can be seen in ZrO_2-modified TaON.[16] The XPS results thus suggested that the trivalent Rh species is the major component in the material.

3.2. Photocatalytic H_2 Evolution from an Aqueous Methanol Solution. Using the as-prepared $BaTiO_3$:Rh samples, photocatalytic water reduction was performed under visible light (λ > 420 nm) in the presence of methanol as an electron donor. Figure 4 shows time courses of H_2 evolution from an aqueous methanol solution using $BaTiO_3$ doped with different amounts of Rh. In this case, Pt was deposited in-situ to offer catalytic sites for water reduction. Undoped $BaTiO_3$ exhibited little photocatalytic activity under visible light, due primarily to its band gap that is too large to harvest visible photons. However, Rh-doped $BaTiO_3$ produced H_2 upon visible light, exhibiting stable performance after an induction period. As summarized in Table 1, the steady rate of H_2 evolution was increased with an increase in the doping amount to reach a maximum at 1.0 mol % doping, beyond which it began to drop. The increase in activity observed in the doping amount from 0 to 1.0 mol % is attributable to an enhanced visible light absorption derived from the doped Rh species, while the activity-drop would be due to the excessively doped Rh species that can work as recombination centers between electrons and holes.[23,25] In all cases, an induction period was observed at the initial stage of the reaction. The induction period is attributable to reduction of higher valence Rh species (e.g., Rh^{4+}) and/or $[PtCl_6]^{2-}$ anions by photogenerated electrons. It is also noted that with increasing the Rh concentration, the induction period tended to become longer, consistent with the idea that the induction period is ascribed to the consumption of photogenerated electrons to reduce Rh^{4+} species (Figure 4).

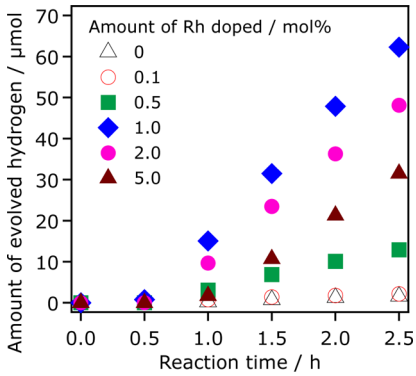

Figure 4. Time courses of H_2 evolution from an aqueous methanol solution using Pt/$BaTiO_3$:Rh with different Rh doping amounts under visible light (λ > 420 nm). Reaction conditions: catalyst, 100 mg; aqueous methanol solution (10 vol%, 100 mL); light source, xenon lamp (300 W) with a cold minor (CM-1) and a cutoff filter; reaction vessel, Pyrex top-irradiation type.

The rate of H_2 evolution over Pt/$BaTiO_3$:Rh was also dependent on the loading amount of Pt, as shown in Figure S2 in the Supporting Information. Although unloaded $BaTiO_3$ exhibited little activity, the activity was enhanced with an increase in the loading amount of Pt to reach a maximum at around 0.3 wt %, and then decreased. The primary role of the loaded Pt is to provide active sites for H_2 evolution.[4] Therefore, the enhanced activity is attributed to an increase in the density of H_2 evolution sites. However, excessively loaded Pt can hinder light absorption of $BaTiO_3$, resulting in a drop in activity. This kind of volcano-like relationship between activity and loading amount of a cocatalyst has been observed in many other heterogeneous systems.[4]

In any of the photoreactions, it is important to examine the dependence of activity on the wavelength of incident light. As shown in Figure 5, the H_2 evolution activity decreased with an increase in the cutoff wavelength of incident light. The longest wavelength available for H_2 evolution was 540 nm, which coincides with the absorption threshold derived from Rh^{3+} dopant. It is thus clear that the photocatalytic activity of $BaTiO_3$:Rh for H_2 evolution results from electron transition from donor levels formed by Rh^{3+} dopant to the conduction band consisting of empty Ti3d orbitals, and that the absorption band above 650 nm, which is due to Rh^{4+} species, does not

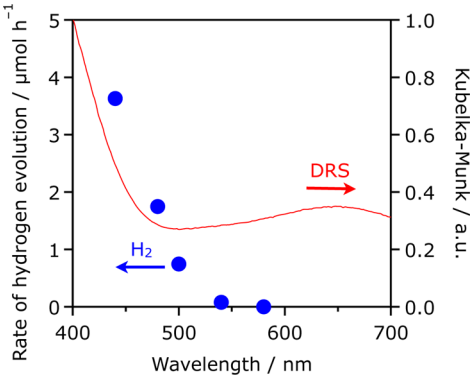

Figure 5. Dependence of the rate of H_2 evolution from an aqueous methanol solution using Pt/$BaTiO_3$:Rh (1.0 mol %) on the cutoff wavelength of incident light. Reaction conditions: catalyst, 25 mg; aqueous methanol solution (10 vol%, 100 mL); light source, xenon lamp (300 W) with a cold minor (CM-1) and a cutoff filter; reaction vessel, Pyrex top-irradiation type. Pt was loaded on $BaTiO_3$:Rh by a photodeposition method, followed by heating in air at 473 K for 1 h.

contribute to H_2 evolution photocatalysis. The apparent quantum yield for H_2 evolution at the optimal condition was calculated to be ca. 0.5% at 420 nm.

Similarly, O_2 evolution reaction was attempted using silver nitrate as an electron acceptor under visible light. However, $BaTiO_3$:Rh did not produce O_2 even when it was combined with colloidal IrO_2 that is one of the most efficient water oxidation cocatalysts.[41] It strongly suggests that the donor level formed by Rh in the forbidden band of $BaTiO_3$ does not host active sites for water oxidation; in other words, the mobility of holes in the donor level is not high enough to oxidize water.

3.3. Comparison with $BaTiO_3$:Rh Prepared by the Solid-State Reaction (SSR) Method. As reported by Kudo et al.,[42] $BaTiO_3$:Rh could be prepared by a conventional SSR method, and exhibited activity for H_2 evolution from an aqueous methanol solution under visible light. As shown in Figure 6, actually, the SSR sample prepared in this study

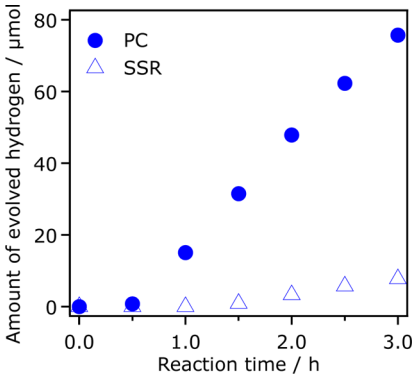

Figure 6. Time courses of H_2 evolution from an aqueous methanol solution using Pt/$BaTiO_3$:Rh (1.0 mol %) prepared by the PC and SSR method under visible light (λ > 420 nm). Reaction conditions: catalyst, 100 mg; aqueous methanol solution (10 vol %, 100 mL); light source, xenon lamp (300 W) with a cold minor (CM-1) and a cutoff filter; reaction vessel, Pyrex top-irradiation type.

exhibited activity for the reaction. However, photocatalytic activity of the SSR sample was much lower than that prepared by the PC method. While no significant difference in XRD pattern, specific surface area and DRS between the PC and SSR sample could be identified (see Figure S3 in the Supporting Information and Table 1), the morphology of these samples was obviously different (Figure 2). The PC sample consists of primary particles of 200−300 nm in size with a relatively smooth surface. On the other hand, the SSR sample is larger agglomerates (>1 μm), consisting of less distinguishable primary particles that possess structural imperfections like grain boundaries. The effect of particle morphology on activity has been reported for $SnNb_2O_6$, which also catalyzes H_2 evolution from aqueous methanol solution under visible light.[43] In that study, it was claimed that smoother and more isolated particles are advantageous for efficient H_2 evolution. Therefore, the less aggregated and smooth morphology of the present PC sample might have a positive impact on activity.

It has been also proposed that SSR involves localized segregation of constituent elements in the final product, generating structural defects during the synthesis, whereas the PC method in principle does not.[34] Such structural imperfections (namely, defects) contribute directly to a decrease in photocatalytic activity, because they act as recombination centers for photogenerated electrons and holes.[1,5] For example, it has been reported that lamellar $KCa_2Nb_3O_{10}$ and restacked $HCa_2Nb_3O_{10}$ nanosheets prepared through the PC method show higher photocatalytic activity for H_2 evolution from an aqueous methanol solution, respectively, than those obtained by the SSR method, even though each sample had almost the same specific surface area.[44,45] Accordingly, it is likely that $BaTiO_3$:Rh prepared by the PC method has lower density of defects than the SSR sample, resulting in a higher rate of H_2 evolution.

3.4. Application to Z-Scheme Water Splitting. Thus, the ability of $BaTiO_3$:Rh to photocatalytically reduce water into H_2 under visible light has been highlighted. The water reduction ability of $BaTiO_3$:Rh was also examined using iodide ion as an electron donor, in which light energy can be stored as chemical energy in the form of H_2 and IO_3^- with a change in the Gibbs energy of 148 kJ mol^{-1}.

$$3H_2O + I^- \rightarrow 3H_2 + IO_3^- \quad (2)$$

In this case, Pt-photodeposited $BaTiO_3$:Rh, dried at 473 K for 1 h in air, was employed. As shown in Figure 7, Pt/$BaTiO_3$:Rh

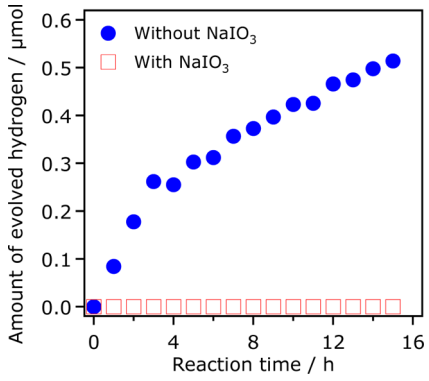

Figure 7. Time courses of H_2 evolution over Pt/$BaTiO_3$:Rh (1.0 mol %) from an aqueous NaI solution in the presence and absence of $NaIO_3$ (1.0 mM) under visible light (λ > 420 nm). Reaction conditions: catalyst, 25 mg; aqueous NaI solution, 100 mL (10 mM); light source, xenon lamp (300 W) fitted with a cold mirror (CM-1) and a cutoff filter (L42); reaction vessel, Pyrex top- irradiation type. Pt was loaded on $BaTiO_3$:Rh by a photodeposition method, followed by heating in air at 473 K for 1 h.

produced H_2 from an aqueous NaI solution under visible light. The rate of H_2 evolution, however, decreased with time due primarily to the accumulation of IO_3^-, which is the oxidation product of I^- (eq 2). Because IO_3^- ions produced were more susceptible to reduction than protons, the forward reaction of H_2 evolution is suppressed with reaction time.[4] When the reaction was conducted in the presence of both I^- (10 mM) and IO_3^- (1.0 mM), no H_2 was produced (square plots, Figure 7), providing evidence for the above competitive model. Nevertheless, this result strongly suggests that $BaTiO_3$:Rh works as a H_2 evolution photocatalyst in a Z-scheme water splitting system using an IO_3^-/I^- shuttle redox mediator.

Figure 8 shows that visible-light-driven Z-scheme water splitting is achievable using Pt/$BaTiO_3$:Rh as a H_2 evolution photocatalyst in combination with a known O_2 evolution photocatalyst of PtO_x/WO_3 in the presence of an IO_3^-/I^- redox couple. Nearly stoichiometric H_2 and O_2 evolution was observable under visible light irradiation, and the amounts increased with time. Here, the oxidation product of IO_3^- ions in the H_2 evolution side were reduced back to I^-, accompanied by

dx.doi.org/10.1021/am405293e | ACS Appl. Mater. Interfaces 2014, 6, 2167−2173

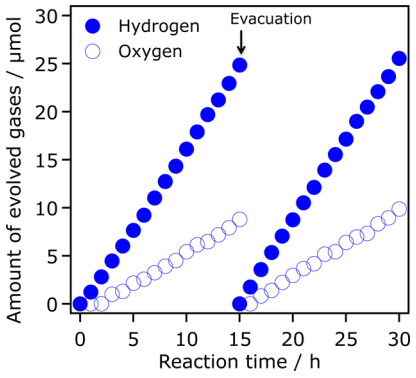

Figure 8. Time course of H_2 and O_2 evolution over a mixture of Pt/$BaTiO_3$:Rh (1.0 mol %) and PtO_x/WO_3 from an aqueous NaI solution under visible light (λ > 420 nm). Reaction conditions: catalyst, 25 mg of Pt/$BaTiO_3$:Rh and 50 mg of PtO_x/WO_3; aqueous solution, 100 mL (10 mM); light source, xenon lamp (300 W) fitted with a cold mirror (CM-1) and a cutoff filter (L42); reaction vessel, Pyrex top-irradiation type. Pt was loaded on $BaTiO_3$:Rh by a photodeposition method, followed by heating in air at 473 K for 1 h.

O_2 evolution, making a catalytic cycle of Z-scheme water splitting.[5] The gas evolution behavior was stable for longer than 30 h of visible light irradiation. Control experiments showed that simultaneous H_2 and O_2 was not observed when one component of the system (Pt/$BaTiO_3$:Rh, PtO_x/WO_3, NaI, light) was absent. These results clearly indicate that Z-scheme water splitting is achieved using a mixture of Pt/$BaTiO_3$:Rh and PtO_x/WO_3 in the presence of an IO_3^-/I^-shuttle redox mediator.

3.5. Application in Photoelectrochemical Cell. Figure 9A shows current−voltage curves for $BaTiO_3$:Rh electrodes with different Rh concentrations under intermittent visible light (λ > 420 nm). Undoped $BaTiO_3$ electrode generated little photocurrent in the potential range examined because of the large band gap, consistent with the result of photocatalytic reaction (Table 1). With increasing the doping amount of Rh, however, cathodic photoresponse was clearly observable, although the absolute photocurrent density was very low (~5 μA cm^{-2}). This cathodic photoresponse could be attributed to water reduction that occurred on the surface of $BaTiO_3$:Rh. As shown in Figure 9B, the cathodic photocurrent was stable, consistent with the results of photocatalytic reactions that indicated the stable behavior of $BaTiO_3$:Rh for visible-light H_2 evolution (Figure 8). These results mean that $BaTiO_3$:Rh behaves as a stable p-type semiconductor for water reduction.

Upon band-gap irradiation (λ > 350 nm), undoped $BaTiO_3$ electrode generated anodic photocurrent assignable to water oxidation, indicating n-type semiconducting property of the material (see Figure S4 in the Supporting Information). Therefore, the p-type semiconducting property of $BaTiO_3$:Rh would be induced by Rh doping. Iwashina and Kudo have reported that substituting a Ti^{4+} site in $SrTiO_3$ with a Rh^{3+} ion without forming oxygen vacancies leads to producing a hole due to charge compensation, changing the semiconducting property of $SrTiO_3$ from n-type to p-type, like Li^+-doped nickel(II) oxide, which is a typical p-type semiconductor.[30] They also suggested that tetravalent Rh species in $SrTiO_3$ are able to release holes because of the reversible nature of Rh^{4+}/Rh^{3+}. It may seem that the origin of p-type semiconducting character of $BaTiO_3$:Rh is similar to $SrTiO_3$:Rh. However, it should be stressed here that doping Rh^{3+} ions into n-type oxide semiconductors does not always give p-type character, as exemplified by $HCa_2Nb_3O_{10}$.[46] The mechanism of how p-type semiconducting property is provided by Rh-doping has yet to be clarified completely, and is now under investigation.

4. CONCLUSION

Rh-doped $BaTiO_3$, prepared by the polymerized complex (PC) method, was shown to achieve the functionality as a p-type semiconductor photocatalyst for H_2 evolution from water containing an electron donor such as methanol or iodide ion under visible light. The PC method produced less aggregated, more smooth particles of $BaTiO_3$:Rh, which exhibited much higher activity than an analogue prepared by a solid-state reaction method. Combining Pt-loaded $BaTiO_3$:Rh with PtO_x/WO_3 achieved stoichiometric water splitting into H_2 and O_2 under visible light according to the Z-scheme principle. $BaTiO_3$:Rh was also found to work as a potential photocathode to produce H_2 from water in a photoelectrochemical cell.

■ ASSOCIATED CONTENT

Supporting Information

Additional characterization and photoelectrochemical data. This material is available free of charge via the Internet at http://pubs.acs.org.

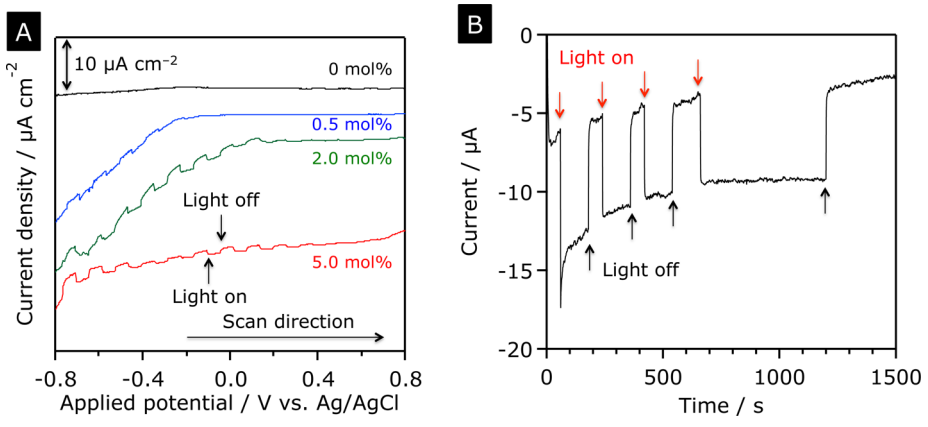

Figure 9. (A) Current−voltage curves in aqueous 0.1 M Na_2SO_4 solution (pH 5.9) under intermittent visible light (λ > 420 nm) for $BaTiO_3$:Rh/FTO electrodes with different Rh doping amounts. Scan rate: 20 mV s^{-1}. (B) Current−time curve for a $BaTiO_3$:Rh (5.0 mol %) electrode (5.25 cm^2) at −0.5 V vs. Ag/AgCl under visible light (λ > 420 nm).

AUTHOR INFORMATION

Corresponding Author

*E-mail: maedak@chem.titech.ac.jp. Tel: +81-3-5734-2239. Fax: +81-3-5734-2284.

Notes

The authors declare no competing financial interest.

ACKNOWLEDGMENTS

The author thanks Profs. Takashi Hisatomi and Kazunari Domen (The University of Tokyo) for assistance in SEM observation and Dr. Yasunori Inoue, Profs. Kiyotaka Nakajima and Michikazu Hara (Tokyo Institute of Technology) for XPS measurement. This work was supported by the PRESTO/JST program "Chemical Conversion of Light Energy" and a Grant-in-Aid for Young Scientists (A) (Project 25709078) as well as a support program for people raising children by the Gender Equality Center (GEC) at the Tokyo Institute of Technology.

REFERENCES

(1) Kudo, A.; Miseki, Y. *Chem. Soc. Rev.* **2009**, *38*, 253−278.
(2) Maeda, K.; Domen, K. *J. Phys. Chem. Lett.* **2010**, *1*, 2655−2661.
(3) Abe, R. *J. Photochem. Photobiol. C: Photochem. Rev.* **2010**, *11*, 179−209.
(4) Maeda, K. *J. Photochem. Photobiol. C: Photochem. Rev.* **2011**, *12*, 237−268.
(5) Maeda, K. *ACS Catal.* **2013**, *3*, 1486−1503.
(6) Sayama, K.; Mukasa, K.; Abe, R.; Abe, Y.; Arakawa, H. *Chem. Commun.* **2001**, 2416−2417.
(7) Abe, R.; Sayama, K.; Sugihara, H. *J. Phys. Chem. B* **2005**, *109*, 16052−16061.
(8) Kato, H.; Hori, M.; Konta, R.; Shimodaira, Y.; Kudo, A. *Chem. Lett.* **2004**, *33*, 1348−1349.
(9) Kato, H.; Sasaki, Y.; Iwase, A.; Kudo, A. *Bull. Chem. Soc. Jpn.* **2007**, *80*, 2457−2464.
(10) Sasaki, Y.; Iwase, A.; Kato, H.; Kudo, A. *J. Catal.* **2008**, *259*, 133−137.
(11) Sasaki, Y.; Nemoto, H.; Saito, K.; Kudo, A. *J. Phys. Chem. C* **2009**, *113*, 17536−17542.
(12) Sasaki, Y.; Kato, H.; Kudo, A. *J. Am. Chem. Soc.* **2013**, *135*, 5441−5449.
(13) Hara, S.; Yoshimizu, M.; Tanigawa, S.; Ni, L.; Ohtani, B.; Irie, H. *J. Phys. Chem. C* **2012**, *116*, 17458−17463.
(14) Abe, R.; Shinmei, K.; Hara, K.; Ohtani, B. *Chem. Commun.* **2009**, 3577−3579.
(15) Abe, R.; Takata, T.; Sugihara, H.; Domen, K. *Chem. Commun.* **2005**, 3829−3831.
(16) Maeda, K.; Terashima, H.; Kase, K.; Higashi, M.; Tabata, M.; Domen, K. *Bull. Chem. Soc. Jpn.* **2008**, *81*, 927−937.
(17) Maeda, K.; Higashi, M.; Lu, D.; Abe, R.; Domen, K. *J. Am. Chem. Soc.* **2010**, *132*, 5858−5868.
(18) Higashi, M.; Abe, R.; Teramura, K.; Takata, T.; Ohtani, B.; Domen, K. *Chem. Phys. Lett.* **2008**, *452*, 120−123.
(19) Matoba, T.; Maeda, K.; Domen, K. *Chem.—Eur. J.* **2011**, *17*, 14731−14735.
(20) Maeda, K.; Lu, D.; Domen, K. *ACS Catal.* **2013**, *3*, 1026−1033.
(21) Tabata, M.; Maeda, K.; Higashi, M.; Lu, D.; Takata, T.; Abe, R.; Domen, K. *Langmuir* **2010**, *26*, 9161−9165.
(22) Kato, H.; Kudo, A. *J. Phys. Chem. B* **2002**, *106*, 5029−5034.
(23) Niishiro, R.; Konta, R.; Kato, H.; Chun, W. J.; Asakura, K.; Kudo, A. *J. Phys. Chem. C* **2007**, *111*, 17420−17426.
(24) Ishii, T.; Kato, H.; Kudo, A. *J. Photochem. Photobiol. A* **2004**, *163*, 181−186.
(25) Konta, R.; Ishii, T.; Kato, H.; Kudo, A. *J. Phys. Chem. B* **2004**, *108*, 8992−8995.
(26) Hwang, D. W.; Kim, H. G.; Lee, J. S.; Kim, J.; Li, W.; Oh, S. H. *J. Phys. Chem. B* **2005**, *109*, 2093−2102.
(27) Nishimoto, S.; Matsuda, M.; Miyake, M. *Chem. Lett.* **2006**, *35*, 308−309.
(28) Iwase, A.; Saito, K.; Kudo, A. *Bull. Chem. Soc. Jpn.* **2009**, *82*, 514−518.
(29) Kumagai, N.; Ni, L.; Irie, H. *Chem. Commun.* **2011**, *47*, 1884−1886.
(30) Iwashina, K.; Kudo, A. *J. Am. Chem. Soc.* **2011**, *133*, 13272−13275.
(31) Matsumoto, Y.; Omae, M.; Sugiyama, K.; Sato, E. *J. Phys. Chem.* **1987**, *91*, 577−581.
(32) Ida, S.; Yamada, K.; Hagiwara, H.; Matsumoto, Y.; Ishihara, T. *J. Am. Chem. Soc.* **2010**, *132*, 17343−17345.
(33) Pechini, M. P. *Ceramic Dielectric Materials*. U.S. Patent 330 697, 1967.
(34) Kakihana, M. *J. Sol−Gel Sci. Technol.* **1996**, *6*, 7−55.
(35) Ma, S. S. K.; Maeda, K.; Abe, R.; Domen, K. *Energy Environ. Sci.* **2012**, *5*, 8390−8397.
(36) Abe, R.; Takata, T.; Sugihara, H.; Domen, K. *Chem. Lett.* **2005**, *34*, 1162−1163.
(37) Kraeutler, B.; Bard, A. J. *J. Am. Chem. Soc.* **1978**, *100*, 4317−4318.
(38) Shannon, R. D. *Acta Crystallogr., Sect. A* **1976**, *32*, 751−767.
(39) Brinen, J. S.; Melera, A. *J. Phys. Chem.* **1972**, *76*, 2525−2526.
(40) Abe, Y.; Kato, K.; Kawamura, M.; Sasaki, K. *Surf. Sci. Spectra* **2001**, *8*, 117−125.
(41) Harriman, A.; Pickering, I. J.; Thomas, J. M.; Christensen, P. A. *J. Chem. Soc., Faraday Trans. 1* **1988**, *84*, 2795−2806.
(42) Konta, R.; Kato, H.; Kudo, A. *Abstr. Chem. Soc. Jpn. Spring Meet.* **2003**, 1PB−062.
(43) Hosogi, Y.; Shimodaira, Y.; Kato, H.; Kobayashi, H.; Kudo, A. *Chem. Mater.* **2008**, *20*, 1299−1307.
(44) Yamashita, Y.; Hyuga, K.; Petrykin, V.; Kakihana, M.; Yoshimura, M.; Domen, K.; Kudo, A. *J. Ceram. Soc. Jpn.* **2007**, *115*, 511.
(45) Maeda, K.; Eguchi, M.; Youngblood, W. J.; Mallouk, T. E. *Chem. Mater.* **2009**, *21*, 3611−3617.
(46) Okamoto, Y.; Ida, S.; Hyodo, J.; Hagiwara, H.; Ishihara, T. *J. Am. Chem. Soc.* **2011**, *133*, 18034−18037.